ADVANCED MATERIALS
www.advmat.de

Multifunctional Quasi-Homogeneous Catalysts as a New Catalytic Strategy to Boost the Performance of Li-O_2 Batteries

Haoran Zhang, Yue Yu, Dongyue Yang, Yingqi Fan, Hao Chen, Ning Zhang, Zhi Wang, Gang Huang, and Xinbo Zhang**

Li-O_2 batteries have been considered as a kind of prospective next-generation batteries due to their ultrahigh energy densities. However, limited capacities, high charge overpotentials, and short lifetime are troubling obstacles for realizing their real-world implementation. Common strategies, including introducing solid-state catalysts (SSCs) and redox mediators (RMs), are insufficient to solve these issues. Herein, Ru-loaded amino-phenanthroline-based carbonized polymer dots (RuApCPDs) integrating the catalytic activity of SSCs with the mobility of RMs have been designed to behave as quasi-homogeneous catalysts in the electrolyte. Their mobile nature can ensure the avoidance of complete coverage of active sites, and the catalytic ability decreases the charge overpotential through co-deposition with the discharge products. Additionally, the RuApCPDs can also adjust the Li^+ solvation structure and well protect the Li metal anodes with high stability. As a result, the introduction of RuApCPDs leads to a fivefold increase in discharge capacity, a low charge voltage of 3.75 V, and a running life of 168 cycles (79 cycles without RuApCPDs). The multifunctional quasi-homogeneous catalyst developed here demonstrates its advantageous potential as a new catalytic strategy for bringing Li-O_2 batteries to become a viable technology.

1. Introduction

Rapid expansion and evolution of portable electronics and electric vehicles require vigorous development of high-energy storage devices. However, lithium-ion batteries (LIBs) are approaching their theoretical energy densities and cannot fulfil the above-increasing demand.[1] Li-O_2 batteries, with an ultrahigh theoretical energy density of 3500 Wh kg^{-1}, have been considered as one of the most promising candidates for next-generation high-energy batteries.[2] Established on the redox reaction between Li metal and oxygen, Li-O_2 batteries have Li_2O_2 as the dominant discharge product on air cathodes during a discharge process, which could be reversely decomposed during the subsequent charge process to release gaseous oxygen ($2Li + O_2 \leftrightarrow Li_2O_2$, $E_0 = 2.96$ V).[3]

At present, despite impressive progress and achievements that have been accomplished in Li-O_2 batteries, challenges and issues brought by the strong oxidizing environment and hard decomposed Li_2O_2 are still hindering the step ahead toward practical application and urgently need to be addressed. The chief concern, briefly speaking, is the poor conductivity nature of solid-state Li_2O_2 that lets the active sites in the cathode side be easily covered by Li_2O_2 to lose activity, and the decomposition of Li_2O_2 requires a large overpotential during the charging process.[4] Thereby, the formation of Li_2O_2 on the surface of cathode hinders the following discharge process, leading to a limited discharge capacity. The high charge voltage would inevitably induce plenty of harmful side reactions, like the degradation of electrolytes and carbon-based cathodes.[5] In order to improve the discharge capacity and reduce the charge voltage, strategies are needed to facilitate the formation and decomposition of Li_2O_2. To this end, solid-state catalysts (SSCs) with catalytic activity toward the oxygen reduction and evolution reactions have been introduced to the air cathodes to reduce the reaction energy barriers.[6] However, owing to the lack of mobility, the continuous accumulation of discharge product would still inevitably result in the complete coverage of active sites (**Figure 1a**), and the decomposition of Li_2O_2 away from the SSCs appears to be powerless, ultimately leading the performance improvement just to a certain extent.[3b,7] Following this, redox mediators (RMs) that could be dissolved into the electrolytes have been developed. RMs have the ability to shuttle electrons through transitions between their reduction/oxidation

H. Zhang, D. Yang, Y. Fan, H. Chen, N. Zhang, Z. Wang, G. Huang, X. Zhang
State Key Laboratory of Rare Earth Resource Utilization
Changchun Institute of Applied Chemistry
Chinese Academy of Sciences
Changchun 130022, China
E-mail: ghuang@ciac.ac.cn; xbzhang@ciac.ac.cn
H. Zhang, D. Yang, Y. Fan, H. Chen, N. Zhang, Z. Wang, G. Huang, X. Zhang
School of Applied Chemistry and Engineering
University of Science and Technology of China
Hefei 230026, China
Y. Yu
Department of Chemistry and Waterloo Institute for Nanotechnology
University of Waterloo
200 University Ave. W.
Waterloo, Ontario N2L 3G1, Canada
The ORCID identification number(s) for the author(s) of this article can be found under https://doi.org/10.1002/adma.202413948

DOI: 10.1002/adma.202413948

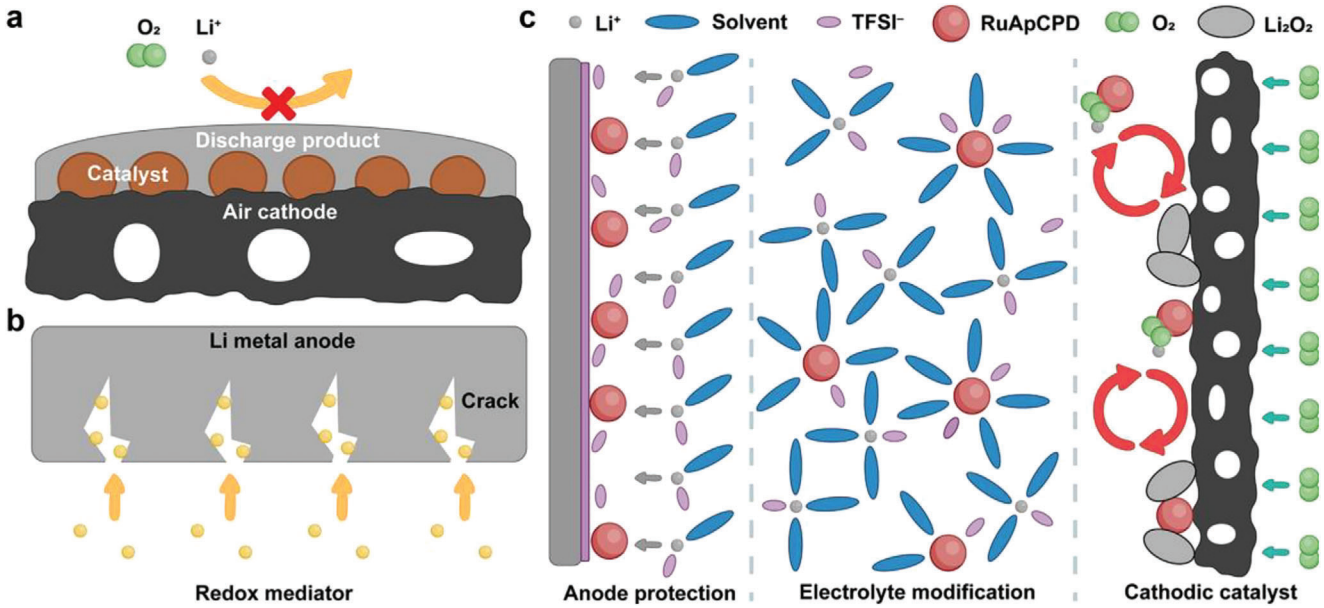

Figure 1. Schematic illustrations of the a) passivation of SSCs, b) Li metal anode corrosion by RMs, and c) RuApCPDs as a multifunctional quasi-homogeneous catalyst in Li-O_2 batteries.

and original states to help generate/decompose Li_2O_2 with an effectively decreased overpotential.[8] Despite the mobile nature makes the coverage of cathode active sites no longer a problem, their shuttle effects would bring side reactions between RMs and Li metal anodes, not to mention the instability of most RMs toward the strong oxidizing environment of Li-O_2 batteries. These bring about the easy degradation of the function of RMs and the continuous loss of active Li (Figure 1b), consequently limiting the long-term operation of batteries.[9] To realize the purpose of facilitating the formation and decomposition of discharge products while circumventing the above-mentioned issues, designing new types of catalysts has unfolded its necessity.

Herein, a quasi-homogeneous catalyst strategy with Ru-loaded amino-phenanthroline-based carbonized polymer dots (RuApCPDs) well-dispersed in the electrolyte has been developed. Besides catalytic ability, RuApCPDs also feature mobility in electrolytes, which prevents the cathode deactivation caused by the coverage of discharge products. The unique features of RuApCPDs make them could boost the discharge process by stabilizing the superoxide intermediates and co-depositing with the discharge products, increasing the discharge capacity fivefold when using bare carbon papers (CPs) as cathodes. In the following charge process, the Li_2O_2 decomposition could be promoted by the catalytic active sites of co-deposited RuApCPDs, reducing the charge voltage from 4.46 to 3.75 V. Additionally, RuApCPDs could also modify the Li^+ solvation structure by reducing the participation of solvent and strengthening that of anions. The Li metal anodes are then well-protected through the generation of stable LiF-rich solid electrolyte interphase (SEI) and the electrostatic shield mechanism. In sum, as illustrated in Figure 1c, RuApCPDs in the electrolyte act as multifunctional roles in Li-O_2 batteries, including cathodic catalyst, electrolyte modification, and anode protection. The integration of these functions makes RuApCPDs enable Li-O_2 batteries with a prolonged cycling time of 168 cycles, surpassing those of batteries without RuApCPDs (79 cycles) or using traditional SSCs (106 cycles).

2. Results and Discussion

2.1. Characterizations of RuApCPDs

In the design of RuApCPDs, two aromatic nitrogen atoms on the amino-phenanthroline (Aphen, Figure S1, Supporting Information) were utilized to coordinate with metal ions to form a stable chelate. The external amino group was selected to form amide bonds that bridged the polymer structure with citric acids (CA), which could also behave as positive charge carriers in the structure of RuApCPDs.[10] In order to introduce efficient catalytic activities for promoting the decomposition of Li_2O_2, Ru^{2+} was selected as the central ion of Aphen chelate. More than that, only the coordination between plural Aphens and Ru^{2+} could form branching structures for polymerization, as illustrated in **Figure 2a**. Accordingly, reactants went through self-assembling, polymerization, and cross-linking to form a polymer intermediate, which subsequently was carbonized to obtain RuApCPDs by solvothermal reaction.[11] Characteristic fluorescence changes in different stages of the synthesis process could shed light on the structure changes (Figure S2, Supporting Information). According to the previous studies of carbonized polymer dots (CPDs),[12] the overall structure of RuApCPDs consists of a central carbonized core and an external polymer shell.

To confirm the basic properties of RuApCPDs, X-ray diffraction (XRD) characterization was first conducted for phase analysis (Figure 2b). The broad peaks at 22.5° and 43° indicate the existence of carbon structure, while no peaks corresponding to crystalline Ru or RuO_2 can be observed after the synthesis.[13] Subsequently, ultraviolet–visible (UV–vis) absorption spectroscopy was

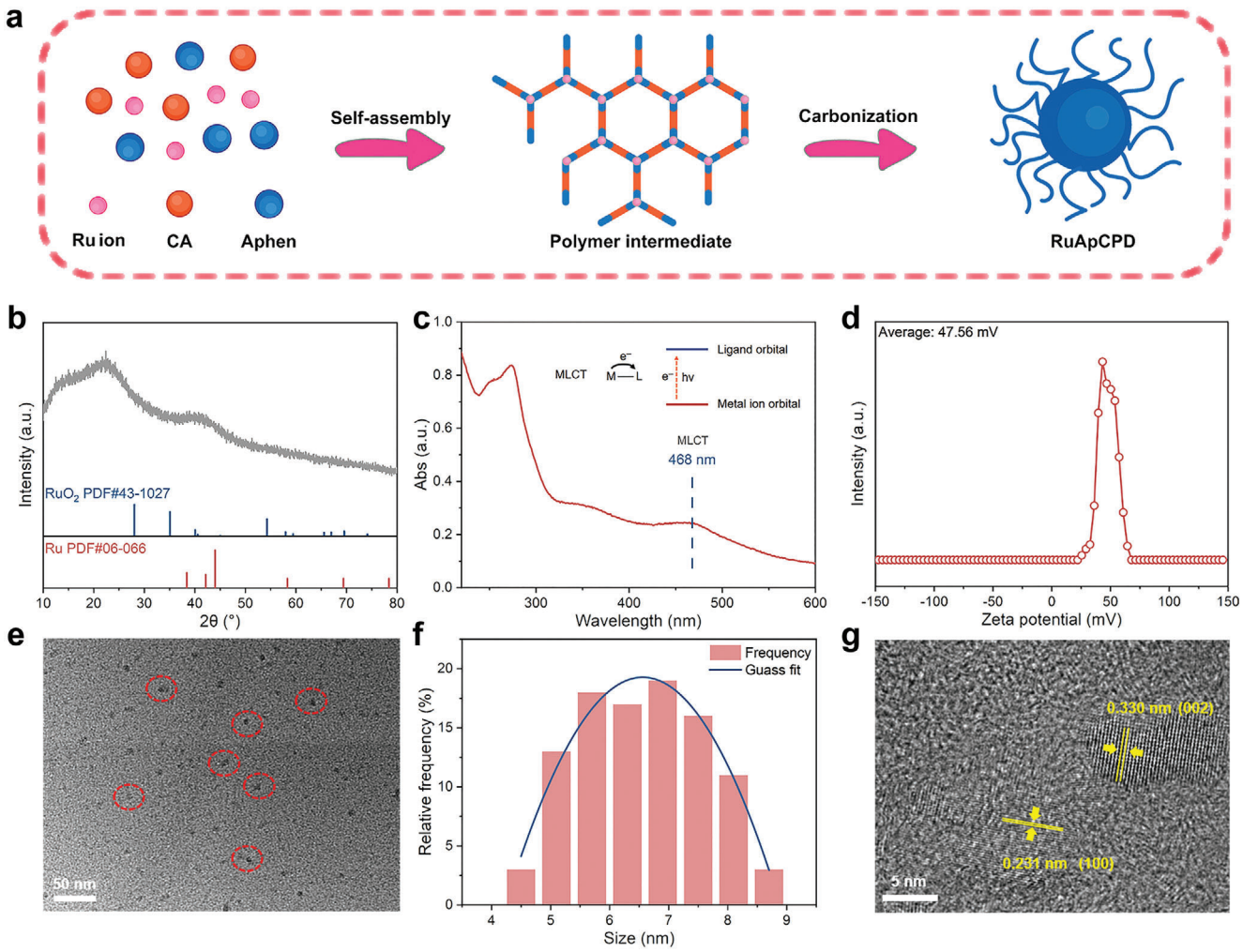

Figure 2. a) Schematic illustration of the preparation procedures for RuApCPDs. Fundamental characterizations of RuApCPDs, including b) XRD, c) UV–vis absorption spectroscopy, d) zeta potential, e) TEM image, f) particle size distribution, and g) HR-TEM image.

performed to detect the coordination between Ru^{2+} and Aphen in RuApCPDs. As shown in Figure 2c, there is an obvious UV–vis absorption peak ≈468 nm when compared to the Aphen and Ru/Aphen (Figure S3, Supporting Information), which can be attributed to the absorption peak from metal-to-ligand charge transfer (MLCT).[14] Then, the zeta potential was measured to study the surface charges of RuApCPDs. Since the Ru^{2+} central ions and the amide groups could act as positive charge carriers, RuApCPDs possess a positive zeta potential with an average value of 47.56 mV (Figure 2d).[10,15] This ensures RuApCPDs with electrostatic interactions with the anions in electrolytes and the ability to behave periodic adsorption/desorption on the electrodes during the charge and discharge processes of Li-O_2 batteries. The nanoscale particle size of RuApCPDs was recorded by transmission electron microscopy (TEM) image. It is clear that the RuApCPDs are evenly dispersed without aggregation (Figure 2e), confirming their minimum sizes for CPDs structures. The sizes of RuApCPDs have been statistically determined, displaying a relatively narrow size distribution with an average value of 6.7 nm (Figure 2f). High-resolution TEM (HR-TEM) image indicates that the lattice spacings of RuApCPDs are 0.231 nm and 0.330 nm (Figure 2g), which are different from those of graphene or graphene quantum dots (0.21 nm for (100) facet and 0.34 nm for (002) facet). This deviation implicates that RuApCPDs are composed of graphene-like core and polymer shell.[16] Note that the polymer structure could hardly be observed due to the lower contrast and drastic degradation under high-energy electron beam in TEM characterization. Instead, dynamic light scattering (DLS) characterization was carried out, which gives a much larger average size than that obtained from TEM images, proving the existence of outer polymer shell (Figure S4, Supporting Information).[16] Ulteriorly, the existence of functional groups on RuApCPDs, especially the amide groups for carrying positive charges,[10,15b] was also confirmed by the Fourier transform infrared (FTIR) spectrum (Figure S5, Supporting Information), revealing the incomplete carbonization of RuApCPDs. With the aim of investigating the surface bonding structures of RuApCPDs, X-ray photoelectron spectroscopy (XPS) was conducted and analyzed (Figure S6, Supporting Information). The high-resolution N 1s spectrum

in Figure S6c (Supporting Information) shows three peaks at 398.3, 399.6, and 399.9 eV, which can be assigned to pyridinic N, N—H bonding, and amide N, respectively,[17] and well reflect the unit fraction stemmed from Aphens and amide bonds for bridging the entire structure. For Ru 3p spectrum (Figure S6d, Supporting Information), it reveals that the Ru has two chemical environments assigned to the Ru^{2+} in the carbonized core and outer polymer shell, respectively. Additionally, high-angle annular dark field scanning transmission electron microscopy (HAADF-STEM) was performed to confirm the distribution of Ru on the carbonized polymer dots. The HAADF-STEM and energy dispersive X-ray (EDX) mapping images confirm a uniform distribution of Ru on the RuApCPDs (Figure S7, Supporting Information).

2.2. Modification of Electrolyte

After getting the basic properties of RuApCPDs, tetraethylene glycol dimethyl ether (TEGDME) and lithium bis(trifluoromethanesulfonyl)imide (LiTFSI) were selected as the supporting electrolyte to conduct further studies. When adding a moderate amount of RuApCPDs into the bare TEGDME solvent, they cannot disperse well even after stirring (Figure S8, Supporting Information). However, once Li salt was added, RuApCPDs could be easily and uniformly dispersed, and consequently, a colloidal electrolyte with a dark brown color was obtained. This phenomenon can be explained by the Derjaguin, Landau, Vervey, and Overbeek (DLVO) theory, which studies the role of ionic strength in establishing colloids' double layer.[18] The addition of Li salt augments the ionic strength of the electrolyte, facilitating the formation of stable double layers that prohibit the aggregation of RuApCPDs. Meanwhile, as typical characteristics of colloids, light scattering phenomenon and Tyndall effect could also be observed for the as-prepared electrolyte (Figure S9a,b, Supporting Information).[19] Notably, no obvious precipitation of RuApCPDs can be found even after 1-month placement, displaying strong stability of the constructed colloidal electrolyte (Figure S9c, Supporting Information). Additionally, the RuApCPDs-added electrolyte could maintain sufficient wettability toward the glass fiber membrane as attested in Figure S10 (Supporting Information).

The influence of the added RuApCPDs on the fundamental properties of electrolytes was then assessed. As shown in **Figure 3**a and S11 (Supporting Information), the ionic conductivity and viscosity of electrolytes are almost unaffected by the amount of RuApCPDs added (0–0.8 wt.%), while the Li^+ transference number experiences a significant increase from 0.561 to 0.731, which can be ascribed to the positive charges of RuApCPDs that electrostatically interact with the anions and consequently restrict their movement. For investigating the solvation structure of electrolytes, nuclear magnetic resonance (NMR) measurement was carried out. Figure 3b manifests that the ^7Li signals continuously shift downfield as the addition amount of RuApCPDs increases, demonstrating that RuApCPDs could weaken the interactions between Li^+ and solvent molecules. Furthermore, the introduction of RuApCPDs also makes ^1H chemical shifts move toward the upfield region (Figure S12, Supporting Information), indicating that there are interactions between RuApCPDs and TEGDME, which accordingly decrease the interactions between Li^+ and TEGDME. To further confirm the interactions between RuApCPDs and TEGDME, linear sweep voltammetry (LSV) was conducted at a scan rate of 0.05 mV s^{-1}. Figure 3c reveals a significant broadening of the electrochemical window due to the decreased highest occupied molecular orbital (HOMO) energy of TEGDME (−7.08 to −8.83 eV) by its interactions with RuApCPDs (Figure S13, Supporting Information). Following this, the stability of RuApCPDs toward superoxide species was examined by checking the UV–vis absorption spectra of the electrolytes treated with KO_2 for different times (Figure 3d; Figure S14, Supporting Information). It is clear that the UV–vis absorption peaks of RuApCPDs at 450 and 387 nm experience no visible changes even after 48 h KO_2 treatment, reflecting their high stability toward the superoxide species. This can be further supported by the ^1H-NMR spectra of RuApCPDs-added electrolytes with well-maintained aromatic structures and bridging skeletons after the addition of KO_2 (Figure S15, Supporting Information). Considering RuApCPDs have interactions with both TEGDME and $TFSI^-$ anions (Figure 3e), molecular dynamics (MD) simulations were performed to study the solvation structure changes of Li^+ (Figure S16, Supporting Information). The radial distribution function (RDF) curves reveal that the addition of RuApCPDs decreases the coordination ratio of TEGDME in the Li^+ solvation structure, while increasing the coordination ratio of $TFSI^-$ (Figure 3f,g). Direct comparisons of the coordination number variation of TEGDME and $TFSI^-$ are presented in Figure S17 (Supporting Information), which clearly points out that the addition of RuApCPDs could enable more $TFSI^-$ to participate in the Li^+ solvation structure and would generate anion-derived SEI films to bring benefits for Li metal anode protection. Overall, RuApCPDs with positive zeta potential and strong antioxidant ability make the electrolyte with increased Li^+ transference number, broadened electrochemical window, and altered Li^+ solvation structure with Li metal anode protection ability.

2.3. Protection of Li Metal Anode

On account of the positive surface charges and modified Li^+ solvation structure, RuApCPDs might play some positive roles on Li metal anode protection. Li-Li symmetric batteries were first assembled to evaluate the anode protection function of RuApCPDs. As shown in Figure S18 (Supporting Information), the introduction of RuApCPDs enables the symmetric battery with a longer and stable cycling performance over 3000 h at 0.1 mA cm^{-2} and 0.1 mAh cm^{-2}. When increasing the cycling current and capacity to 0.3 mA cm^{-2} and 0.3 mAh cm^{-2}, the performance improvement becomes more obvious. RuApCPDs make the battery deliver a more than four times longer cycle life than the battery without RuApCPDs (**Figure** 4a), highlighting the effective protection ability of RuApCPDs toward the Li metal anode. To shed light on the mechanisms of Li metal anode protection, XPS characterization of cycled Li metal anodes in symmetric batteries was conducted. As indicated in Figure 4b, the introduction of RuApCPDs could induce the formation of a LiF-rich SEI film on the Li metal surface, which is commonly considered as a beneficial component of Li metal anode protection.[20] Generating such

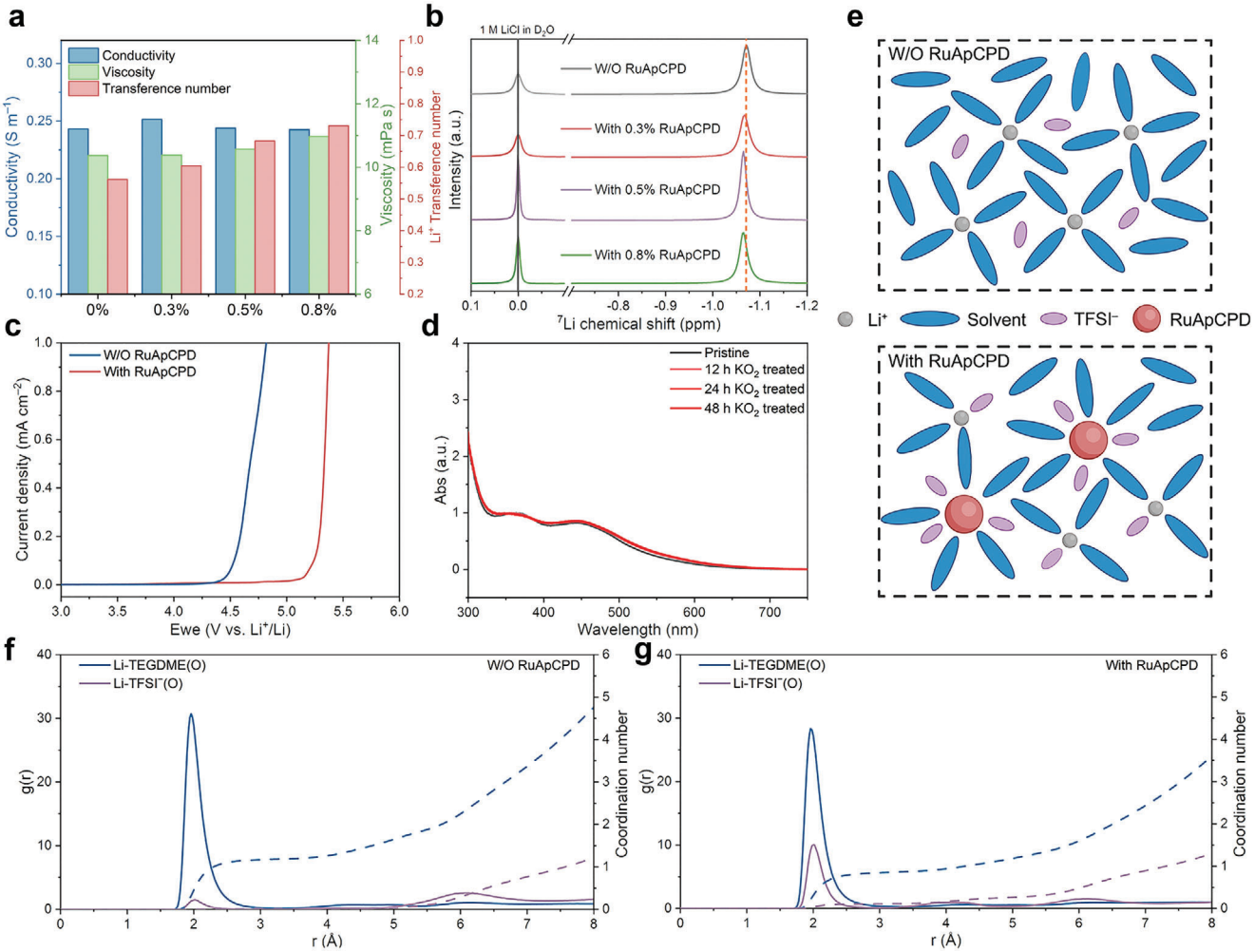

Figure 3. a) Ionic conductivities, viscosities, and Li^+ transference numbers of electrolytes with varied concentrations of RuApCPDs. b) ^{7}Li-NMR spectra of electrolytes with varied concentrations of RuApCPDs. c) LSV curves of electrolytes without (W/O) and with RuApCPDs. d) UV–vis absorption spectra of RuApCPDs-added electrolytes under different times of KO_2 treatment. e) Schematic illustrations of Li^+ solvation structures W/O and with RuApCPDs. Calculated RDF curves and coordination numbers of electrolytes: f) W/O and g) with RuApCPDs.

a kind of SEI is a result of coordination augmentation of $TFSI^-$ in the Li^+ solvation structure, plus RuApCPDs attracting $TFSI^-$ with their positive surface charges. Thereby, more $TFSI^-$ anions are able to be decomposed on the surface of the Li metal anode during battery cycling. Meanwhile, in Figure 4c, the growth trend of interfacial impedance of Li-Li symmetric battery with RuApCPDs is much slower than that of battery with bare electrolyte, further proving that the RuApCPDs enable the generation of a stable SEI film to suppress side reactions between the electrolyte and Li metal anode. Besides acting as a stable interfacial layer, the LiF-rich SEI film could also regulate the Li plating and stripping behavior. As demonstrated in Figure 4d, and Figures S19, S20 (Supporting Information), Li metal anodes of symmetric batteries W/O RuApCPDs exhibit rough, cracked surfaces and fluffy cross-sections just after ten cycles, as a sign of uneven Li plating and stripping. In comparison, Li metal anodes from RuApCPDs-based symmetric batteries display smooth and compact surfaces and cross-sections even after 40 cycles (Figure S20, Supporting Information). Except for the function of LiF-rich SEI film, this uniform Li plating and stripping can also be accounted by the electrostatic shield mechanism brought by the positively charged RuApCPDs.[21] Due to the large sizes, RuApCPDs could enable strong electrostatic repulsion forces toward cations at a large scale, which prohibits the local aggregation of Li^+ and consequently guarantees uniform distribution of Li^+ at the surface of Li metal anode. Importantly, different from conventional RMs, RuApCPDs do not act as a kind of electron shuttle that is highly reactive toward Li metal anodes, so avert the troubling shuttle effects induced Li metal anode corrosion and catalyst consumption. As an experimental verification, SEM images of Li metal anodes from cycled Li-O_2 batteries with RM or RuApCPDs were acquired. It is evident that the Li metal anode is eroded severely by the LiBr-based RM, leaving apparent cracks on the Li metal surface (Figure 4e), while the Li metal anode cycled in the RuApCPDs-based battery possesses a relatively smooth surface without observable splits (Figure 4f). This result demonstrates the obvious superiority of RuApCPDs over conventional RMs.

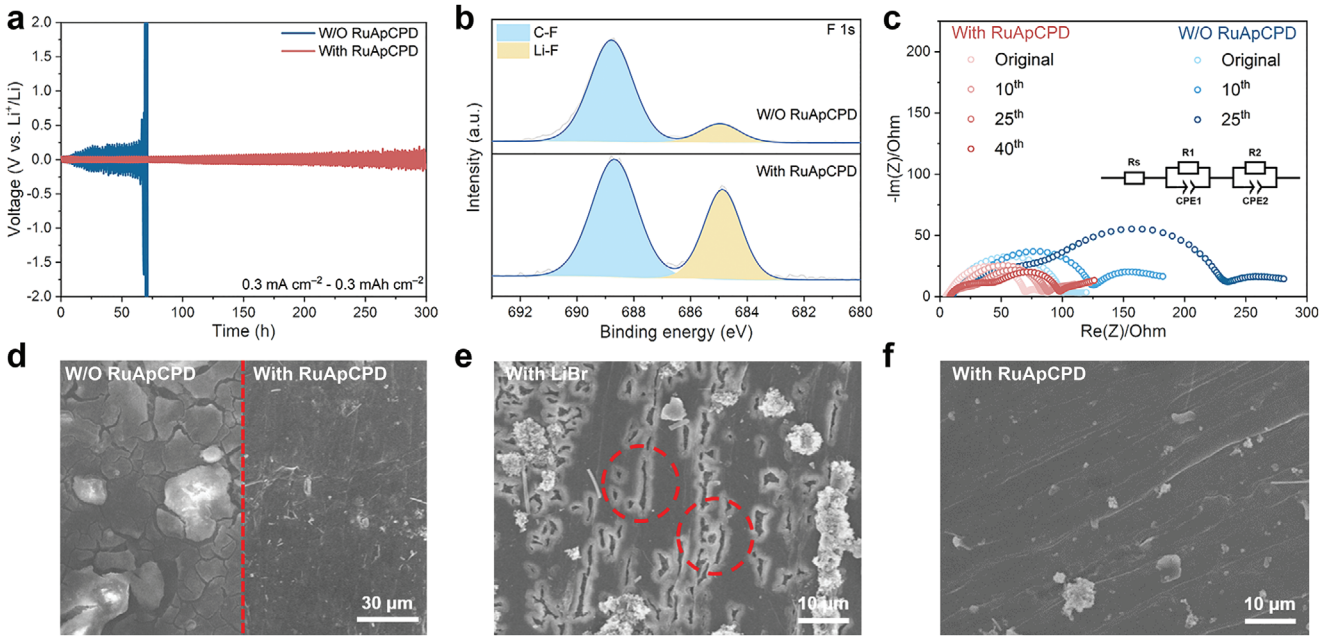

Figure 4. a) Cycling performance of Li-Li symmetric batteries W/O and with RuApCPDs. b) F 1s XPS spectra of Li metal anodes in cycled Li-Li symmetric batteries. c) EIS spectra of Li-Li symmetric batteries at different cycle states. d) SEM images of the 25th cycle Li metal anodes in Li-Li symmetric batteries W/O and with RuApCPDs. SEM images of Li metal anodes in Li-O_2 batteries with e) LiBr and f) RuApCPDs at the 10th cycle.

2.4. Facilitating Formation and Decomposition of Li_2O_2

Apart from the benefits brought to the electrolyte and anode, RuApCPDs could also behave as quasi-homogeneous catalysts to promote the formation and decomposition of Li_2O_2. To begin with, for the prime exploration of the discharge process, in situ pressure monitoring was conducted to check whether the introduction of RuApCPDs would alter the $2e^-$ discharge reaction of Li-O_2 batteries by calculating the consumption ratio of electron and oxygen (**Figure** 5a). The value is calculated to be e^-/O_2 = 1.92, which together with the negligible discharge capacity under the Ar atmosphere and barely unchanged open circuit voltage (Figure S21, Supporting Information) certify that the RuApCPDs-added Li-O_2 batteries still follow a two-electron discharge reaction with Li_2O_2 as the discharge product. As a direct identification of discharge product, XRD patterns of the discharged air cathode in RuApCPDs-added Li-O_2 batteries show evident diffraction peaks of Li_2O_2, which can be reversibly decomposed during the following recharge process (Figure 5b). The morphology of the discharge product was confirmed to be typical toroidal-shape Li_2O_2 in RuApCPDs-added Li-O_2 batteries (Figure S22, Supporting Information). The differential electrochemical mass spectrometry (DEMS) technique was also used to check the reversible decomposition of Li_2O_2 during a charging process. The evolution of O_2 can be detected (Figure S23, Supporting Information), providing convincing evidence for the dissociation of Li_2O_2 below 4 V. These results demonstrate that the RuApCPDs-added Li-O_2 batteries follow the typical $2e^-$ electrochemical reactions with the highly reversible formation and decomposition of Li_2O_2.

To directly illustrate the catalytic function of RuApCPDs, CPs loaded with RuApCPDs (C-RuApCPD) were prepared as contrast cathodes to eliminate the influence of electrolyte solvation effect and anode protection. Although C-RuApCPD cannot significantly reduce the discharge overpotential like adding RuApCPDs into the electrolyte, it has the ability to markedly increase the discharge current (Figure 5c, the electrolytes and electrodes of the Li-O_2 batteries have been summarized in Table S1, Supporting Information). This demonstrates that RuApCPDs alone can accelerate the discharge reaction kinetics to promote the formation process of Li_2O_2. For dispersing RuApCPDs into the electrolyte, their mobility together with the electrostatic interactions from Ru^{2+} and amide groups enable a better stabilization effect on superoxide anions, resulting in a decreased discharge overpotential. During the charging process, batteries with C-RuApCPD and RuApCPDs both display a lower charge voltage peak at 3.25 V when compared to the battery without RuApCPDs (3.5 V), manifesting the well-catalytic ability of RuApCPDs on facilitating Li_2O_2 decomposition. The RuApCPDs enabled large charge current can be attributed to the synergistic effects of their intrinsic catalytic activity and mobile nature in the electrolyte that can continuously catalyze the decomposition of Li_2O_2. The 1st cycle discharge and charge curves of Li-O_2 batteries W/O and with RuApCPDs are displayed in Figure S24a (Supporting Information). It is obvious that the terminal charge voltage can be reduced from 4.46 to 4.12 V when using C-RuApCPD and further reduced to 3.75 V when adding RuApCPDs into the electrolyte. In addition, the longer cycle life of Li-O_2 battery using C-RuApCPD than that using CNTs also proves the intrinsic catalytic ability of RuApCPDs toward the formation and decomposition of Li_2O_2 (Figure S24b, Supporting Information). As another verification of whether RuApCPDs in the electrolyte have the ability to directly catalyze the discharge and charge processes, the electrochemical performance of bare CPs-based Li-O_2 batteries W/O and with RuApCPDs in the electrolytes were compared (Figure S25,

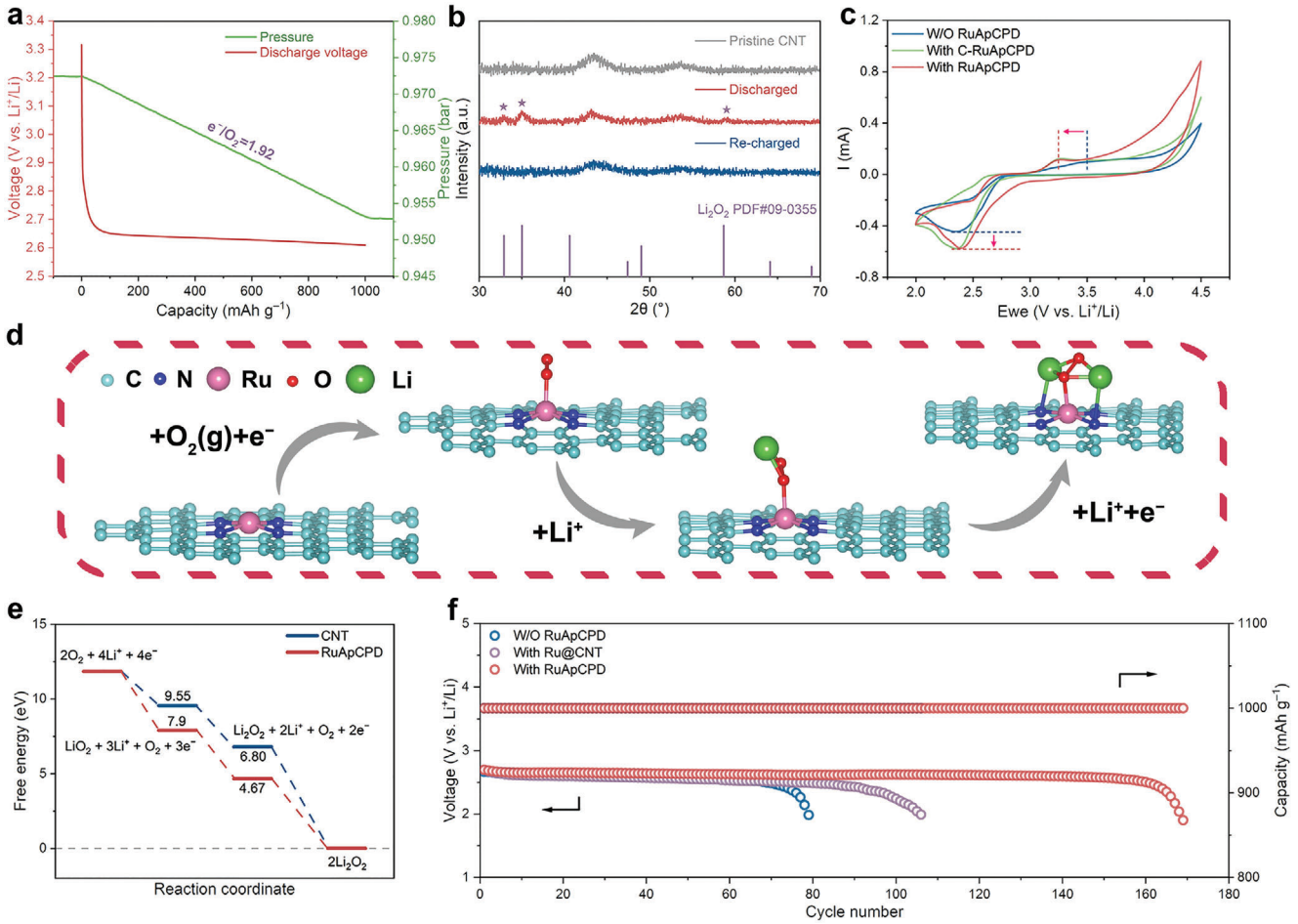

Figure 5. a) In situ pressure monitoring of Li-O_2 batteries with RuApCPDs during a discharge process. b) XRD patterns of pristine, discharged, and re-charged air cathodes in Li-O_2 batteries with RuApCPDs. c) CV curves of Li-O_2 batteries at a scan rate of 1 mV s^{-1}. d) Schematic illustration of the formation process of Li_2O_2 on RuApCPDs. e) Free energy calculations of Li_2O_2 formation on CNTs and RuApCPDs. f) Cycling performance of Li-O_2 batteries at 500 and 1000 mAh g^{-1}.

Supporting Information). In the full cycling assessment, the significantly decreased discharge and charge overpotentials together with the impressive fivefold enlargement of discharge capacity suggest that, besides the superoxide stabilization effect, RuApCPDs can individually act as cathodic catalysts through co-deposition with Li_2O_2 on the air cathodes, offering extra reaction sites for Li_2O_2 growth and decomposition and thus promoting the discharge and charge processes (Figure S25a, Supporting Information). Consequently, the bare CPs-based Li-O_2 batteries with RuApCPDs exhibit a cycle life of 118 cycles, much longer than the five cycles delivered by batteries W/O RuApCPDs (Figure S25b, Supporting Information). Further experimental elucidation of the co-deposition of RuApCPDs and Li_2O_2 was carried out in Li-O_2 batteries with nanoporous gold (NPG) cathodes. The high-resolution N 1s spectrum of the discharged NPG cathode displays three characteristic peaks from RuApCPDs (Figure S26a, Supporting Information), as proof of RuApCPDs co-depositing with Li_2O_2. During the charge process, the deposited products can be completely removed accompanied by the detachment of RuApCPDs from the NPG surface, leaving the NPG porous structure again (Figure S26b–d, Supporting Information). To sum up, RuApCPDs with Ru^{2+} active sites, positive charges, and mobile nature concurrently function together to interact with superoxide intermediates, co-deposit with Li_2O_2, and accelerate the formation and decomposition of Li_2O_2.

DFT calculations were then applied to further clarify the functions of RuApCPDs on the cathode side of Li-O_2 batteries. As shown in Figure S27 (Supporting Information), RuApCPDs exhibit absorption energies of −1.78 and −3.72 eV toward the superoxide anion and Li_2O_2, respectively, much larger than those of CNTs (−0.04 and −1.50 eV). This suggests that RuApCPDs possess the ability to stabilize superoxide and together with their mobile nature to co-deposit with Li_2O_2 rather than the direct formation of Li_2O_2 on the CNTs surfaces during the discharge process. After this, free energy changes during the discharge process were calculated to elucidate the discharge reaction paths on CNTs and RuApCPDs.[22] For RuApCPDs, superoxide intermediates are first stabilized through the interactions with Ru^{2+} active sites, and then the N on RuApCPDs facilitates the binding of Li^+ to the superoxide and ultimately generates Li_2O_2 (Figure 5d). It can be seen from Figure 5e that the formation of LiO_2 intermediates and Li_2O_2 on RuApCPDs are thermodynamically more

favorable than on CNTs, indicating that Li_2O_2 prefers to generate together with RuApCPDs. Besides the benefits brought to the discharge process, in conjunction with their co-deposition behavior, catalytic ability, and mobile nature that CNTs do not have, RuApCPDs could also perform well during the charging process.

2.5. Comprehensive Performance Improvement of Li-O_2 Batteries

Considering the positive functions of RuApCPDs on the cathode, electrolyte, and Li metal anode of Li-O_2 batteries, detailed full-cell performance was studied. As illustrated in Figure S28 (Supporting Information), the addition of RuApCPDs into the electrolyte brings enhancement to the discharge process with a large specific capacity of 7263 mAh g^{-1} and charge process with decreased overpotentials, much better than the batteries with traditional SSCs. For the long-term cycling performance (Figure 5f), RuApCPDs make Li-O_2 batteries deliver a prolonged cycle life of 168 cycles, ≈2.1 and 1.6 times the lives of batteries without RuApCPDs (79 cycles), and with traditional SSCs (106 cycles). In addition, RuApCPDs could also endow Li-O_2 batteries with improved rate capability and cycling stability (Figure S29, Supporting Information). It should be mentioned that even after 25 cycles, 80% of RuApCPDs still remain in the electrolyte (Figure S30, Supporting Information), revealing their continued positive effects on the key components of Li-O_2 battery, which in turn improves the overall battery performance.

3. Conclusion

In summary, by endowing CPDs with Ru^{2+} catalytic active sites, quasi-homogeneous catalysts RuApCPDs that could be well dispersed in the electrolyte have been developed, which integrate the catalytic activity of SSCs and mobility of RMs together. During the discharge process, RuApCPDs in the electrolyte have the ability to decrease overpotential and increase discharge capacity by stabilizing the superoxide intermediates and co-depositing with Li_2O_2. The co-deposited RuApCPDs could thereby continuously catalyze the decomposition of Li_2O_2 in the charging process with their Ru^{2+} catalytic active sites and mobile nature, decreasing the terminal charge voltage from 4.46 to 3.75 V. Furthermore, RuApCPDs could also modify the electrolyte with increased Li^+ transference number, broadened electrochemical window, and $TFSI^-$ participated Li^+ solvation structure. The $TFSI^-$ derived LiF-rich SEI film and positively charged RuApCPDs rendered electrostatic shield mechanism well protect the Li metal anodes with stable interfacial layer and uniform and corrosion-free plating/stripping behavior, circumventing the shuttle effects induced Li metal anode corrosion by traditional RMs. Benefiting from the above advantageous features, RuApCPDs comprehensively improve the electrochemical performance of Li-O_2 batteries, like increased discharge capacity (fivefold increase with CPs as cathodes), prolonged lifetime (168 cycles vs 79 cycles without RuApCPDs), and enhanced rate capacity (4892 mAh g^{-1} at 1000 mA g^{-1}). All in all, with catalytic ability and mobility, the quasi-homogeneous catalyst developed here encapsulates the benefits of SSCs and RMs while discarding their drawbacks, offering a brand-new catalyst designing strategy for promoting the performance of Li-O_2 batteries.

Supporting Information

Supporting Information is available from the Wiley Online Library or from the author.

Acknowledgements

H.Z. and Y.Y. contributed equally to this work. The authors thank the financially supported by the National Key R&D Program of China (2021YFF0500600), National Natural Science Foundation of China (U23A20575, U22A20437, 52171194, 52271140, 22209138), New Cornerstone Science Foundation through the XPLORER PRIZE, Strategic Priority Research Program of the Chinese Academy of Sciences (Grant No. XDB1040101), Guangdong Basic and Applied Basic Research Foundation (2021A1515110464), and National Natural Science Foundation of China Outstanding Youth Science Foundation of China (Overseas).

Conflict of Interest

The authors declare no conflict of interest.

Data Availability Statement

The data that support the findings of this study are available from the corresponding author upon reasonable request.

Keywords

carbonized polymer dots, Li-O_2 batteries, multifunctional catalysts, performance improvement, quasi-homogeneous catalysts

Received: September 16, 2024
Revised: November 30, 2024
Published online:

[1] a) J. G. Zhang, W. Xu, J. Xiao, X. Cao, J. Liu, *Chem. Rev.* **2020**, *120*, 13312; b) S. H. Jiao, X. D. Ren, R. G. Cao, M. H. Engelhard, Y. Z. Liu, D. H. Hu, D. H. Mei, J. M. Zheng, W. G. Zhao, Q. Y. Li, N. Liu, B. D. Adams, C. Ma, J. Liu, J. G. Zhang, W. Xu, *Nat. Energy.* **2018**, *3*, 739; c) X.-T. Li, J. Chou, Y.-H. Zhu, W.-P. Wang, S. Xin, Y.-G. Guo, *eScience.* **2023**, *3*, 100121.

[2] a) W. J. Kwak, Rosy, D. S., C. Xia, H. Kim, L. R. Johnson, P. G. Bruce, L. F. Nazar, Y. K. Sun, A. A. Frimer, M. Noked, S. A. Freunberger, D. Aurbach, *Chem. Rev.* **2020**, *120*, 6626; b) Y. Liu, J. Cai, J. Zhou, Y. Zang, X. Zheng, Z. Zhu, B. Liu, G. Wang, Y. Qian, *eScience.* **2022**, *2*, 389; c) Y. Dou, X.-G. Wang, D. Wang, Q. Zhang, C. Wang, G. Chen, Y. Wei, Z. Zhou, *Chem. Eng. J.* **2021**, *409*, 128145; d) X. Zheng, M. Yuan, Y. Zhao, Z. Li, K. Shi, H. Li, G. Sun, *Adv. Energy Mater.* **2023**, *13*, 2204019.

[3] a) J. H. Kang, J. Lee, J. W. Jung, J. Park, T. Jang, H. S. Kim, J. S. Nam, H. Lim, K. R. Yoon, W. H. Ryu, I. D. Kim, H. R. Byon, *ACS Nano.* **2020**, *14*, 14549; b) Y. Wang, Y. C. Lu, *Energy Storage Mater.* **2020**, *28*, 235.

[4] a) Q. Lv, Z. Zhu, S. Zhao, L. Wang, Q. Zhao, F. Li, L. A. Archer, J. Chen, *J. Am. Chem. Soc.* **2021**, *143*, 1941; b) B. He, G. Li, J. Li, J. Wang, H. Tong, Y. Fan, W. Wang, S. Sun, F. Dang, *Adv. Energy Mater.* **2021**, *11*, 2003263; c) Z. Zhao, X. Zhang, Z. Zhou, E. Wang, Z. Peng, *Nano Lett.* **2021**, *22*, 501; d) X. Zheng, M. Yuan, D. Guo, C. Wen, X. Li, X. Huang, H. Li, G. Sun, *ACS Nano.* **2022**, *16*, 4487.

[5] a) P. Zhang, M. Ding, X. Li, C. Li, Z. Li, L. Yin, *Adv. Energy Mater.* **2020**, *10*, 2001789; b) C. Dang, Q. Mu, X. Xie, X. Sun, X. Yang, Y. Zhang, S. Maganti, M. Huang, Q. Jiang, I. Seok, W. Du, C. Hou, *Adv. Compos. Hybrid Mater.* **2022**, *5*, 606.

[6] Y. Zhou, S. Guo, *eScience* **2023**, *3*, 100123.
[7] Q. Qiu, J. Long, P. Yao, J. Wang, X. Li, Z.-Z. Pan, Y. Zhao, Y. Li, *Catal. Today.* **2023**, *420*, 114138.
[8] Y. Y. Dou, Z. J. Xie, Y. J. Wei, Z. Q. Peng, Z. Zhou, *Natl. Sci. Rev.* **2022**, *9*, nwac040.
[9] a) L. L. Fan, M. Li, X. F. Li, W. Xiao, Z. W. Chen, J. Lu, *Joule.* **2019**, *3*, 361; b) B. Lin, Y. Zhang, W. Li, J. Huang, Y. Yang, S. W. Or, Z. Xing, S. Guo, *eScience.* **2024**, *4*, 100180.
[10] Y. Wu, H. Wei, H. C. van der Mei, J. de Vries, H. J. Busscher, Y. Ren, *Mater. Today Bio.* **2021**, *12*, 100151.
[11] S. Y. Lu, L. Z. Sui, J. J. Liu, S. J. Zhu, A. M. Chen, M. X. Jin, B. Yang, *Adv. Mater.* **2017**, *29*, 1603443.
[12] Y. B. Song, S. J. Zhu, J. R. Shao, B. Yang, *J. Polym. Sci., A: Polym. Chem.* **2016**, *55*, 610.
[13] a) G. Sun, X. Li, Y. Qu, X. Wang, H. Yan, Y. Zhang, *Mater. Lett.* **2008**, *62*, 703; b) L. L. Yue, H. L. Li, Q. Sun, J. Zhang, X. G. Luo, F. S. Wu, X. J. Zhu, *ACS Appl. Nano Mater.* **2020**, *3*, 869.
[14] J. Zhao, W. Li, S. Gou, S. Li, S. Lin, Q. Wei, G. Xu, *Inorg. Chem.* **2018**, *57*, 8396.
[15] a) V. B. Kumar, R. Kumar, A. Gedanken, O. Shefi, *Ultrason. Sonochem.* **2019**, *52*, 205; b) I. Ostolska, M. Wiśniewska, *Colloid Polym. Sci.* **2014**, *292*, 2453.
[16] J. J. Liu, Y. J. Geng, D. W. Li, H. Yao, Z. P. Huo, Y. F. Li, K. Zhang, S. J. Zhu, H. T. Wei, W. Q. Xu, J. L. Jiang, B. Yang, *Adv. Mater.* **2020**, *32*, 1906641.
[17] R. Arrigo, M. Hävecker, S. Wrabetz, R. Blume, M. Lerch, J. McGregor, E. P. J. Parrott, J. A. Zeitler, L. F. Gladden, A. K. Gericke, R. Schlögl, D. S. Su, *J. Am. Chem. Soc.* **2010**, *132*, 9616.
[18] T. Missana, A. Adell, *J. Colloid Interface Sci.* **2000**, *230*, 150.
[19] a) W. C. Xiao, Z. H. Deng, J. K. Huang, Z. H. Huang, M. M. Zhuang, Y. L. Yuan, J. F. Nie, Y. Zhang, *Anal. Chem.* **2019**, *91*, 15114; b) Z. Meng, Z. Qiu, Y. Shi, S. Wang, G. Zhang, Y. Pi, H. Pang, *eScience.* **2023**, *3*, 100092.
[20] a) Z. Y. Han, C. Zhang, Q. W. Lin, Y. B. Zhang, Y. Q. Deng, J. W. Han, D. C. Wu, F. Y. Kang, Q. H. Yang, W. Lv, *Small Methods.* **2021**, *5*, 2001035; b) Y. Yang, W. Yang, H. Yang, H. Zhou, *eScience.* **2023**, *3*, 100170.
[21] a) F. Ding, W. Xu, G. L. Graff, J. Zhang, M. L. Sushko, X. L. Chen, Y. Y. Shao, M. H. Engelhard, Z. M. Nie, J. Xiao, X. J. Liu, P. V. Sushko, J. Liu, J. G. Zhang, *J. Am. Chem. Soc.* **2013**, *135*, 4450; b) Z. Wang, M. Zhou, L. Qin, M. Chen, Z. Chen, S. Guo, L. Wang, G. Fang, S. Liang, *eScience.* **2022**, *2*, 209.
[22] X. Hu, G. Luo, Q. Zhao, D. Wu, T. Yang, J. Wen, R. Wang, C. Xu, N. Hu, *J. Am. Chem. Soc.* **2020**, *142*, 16776.